Editors' Suggestion

Magnetic Exciton of EuS Revealed by Resonant Inelastic X-Ray Scattering

Lucia Amidani*
The Rossendorf Beamline (ROBL) at the ESRF, 71 Avenue des Martyrs, Grenoble 38043, France and Institute of Resource Ecology, Helmholtz-Zentrum Dresden-Rossendorf (HZDR), Bautzner Landstraße 400, 01328 Dresden, Germany

Jonas J. Joos
LumiLab, Department of Solid State Sciences, Ghent University, Krijgslaan 281-S1, B-9000 Gent, Belgium and Antwerp Maritime Academy, Noordkasteel Oost 6, Antwerp 2030, Belgium

Pieter Glatzel
ESRF—The European Synchrotron, 71 Avenue des Martyrs, 38000 Grenoble, France

Jindřich Kolorenč†
Institute of Physics (FZU), Czech Academy of Sciences, Na Slovance 2, 182 00 Prague, Czech Republic

(Received 30 October 2023; revised 15 July 2024; accepted 11 December 2024; published 27 January 2025)

We report the valence-to-core resonant inelastic x-ray scattering of EuS measured at the L_3 edge of Eu. The obtained data reveal two sets of excitations: one set is composed of a hole in the S 3p bands and an electron excited to extended Eu 5d band states, and the other is made up from a hole in the Eu 4f states and an electron in localized Eu 5d states bound to the 4f hole by its Coulomb potential. The delocalized excitations arise from the dipole-allowed 5d → 2p emissions, whereas the localized excitations result from the dipole-forbidden (quadrupole-allowed) 4f → 2p emissions. Both these emission channels have a comparable intensity thanks to a small number of occupied 5d states (≈0.6) combined with a large number of occupied 4f states (seven). We identify the localized electron-hole pairs with the "magnetic excitons" suggested in the past as an interpretation of the sharp features seen in the optical absorption spectra. Our observations provide a direct experimental evidence of these excitons, which has been missing up to now.

DOI: 10.1103/PhysRevLett.134.046401

Europium sulfide belongs to the europium monochalcogenides series (EuX, X = O, S, Se, Te), which represents a rare example of intrinsic magnetic semiconductors [1]. EuX crystallize in the rock salt structure, with the Eu^{2+} ions having a half filled 4f shell ($4f^7$ configuration) and carrying purely spin magnetic moment, thanks to which EuX can serve as prototypes of Heisenberg magnets. The semiconducting gap is found between the occupied 4f states and the empty conduction band of predominantly Eu 5d character, while the S 3p states constitute the occupied valence band located below the occupied 4f states [1].

The discovery of the Eu monochalcogenides in the 1960s [2] elicited a strong scientific interest since the coexistence of their semiconducting and magnetic properties was promising for spintronics and magneto-optics applications [2]. When it became clear that doping could not raise the Curie temperature up to room temperature, the interest in EuX turned toward more fundamental studies. In the last two decades, EuX attracted renewed attention thanks to the discovery of new properties, like those of EuX nanoparticles intended for magneto-optical devices [3–6], the interface magnetism induced by coupling EuX with a topological insulator [7], the possibility to raise the Curie temperature in strained multilayered structures [8,9], or the demonstration that optical control can be used to induce EuX magnetization on the ultrafast timescale [10–12].

The new developments stimulated further fundamental investigations, focusing in particular on the changes of the electronic structure across the Curie temperature aimed to understand the exchange mechanism responsible for the ferromagnetic ordering [13–16]. Less attention has been paid to an unsettled debate about the interpretation of the optical absorption. The absorption spectrum of EuX is characterized by two peaks, the first being located at the onset and the second on the rising edge of the spectrum [17]. While there is a general consensus that these peaks originate from transitions, in which a 4f electron is excited to the crystal-field-split $5d(t_{2g})$ and $5d(e_g)$ states, the spatial extent of these excited states is debated.

The interpretation proposed by Wachter and collaborators assumes that the excited electron is itinerant and resides in a *delocalized* single-particle Bloch state.

*Contact author: lucia.amidani@esrf.fr
†Contact author: kolorenc@fzu.cz

 © 2025 American Physical Society

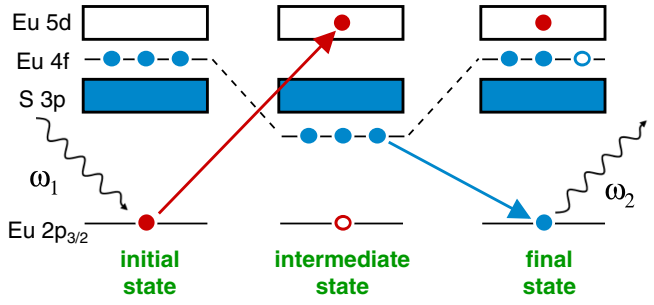

FIG. 1. Scheme of the RIXS process. The incoming photon ω_1 excites a core electron to an unoccupied state. Then, a valence electron decays and fills the core hole, releasing the excess energy by emitting photon ω_2. As a result, a valence electron is promoted to the conduction band.

The shape of the absorption spectrum then implies that the 5d bands are very narrow, with their width being smaller than the crystal-field splitting [17]. This picture was criticized by Kasuya and collaborators who argue that the Coulomb attraction of the hole created in the localized 4f shell prevents the excited electron from leaving the atom. Instead, *localized* many-body states $4f^6 5d^1(t_{2g})$ and $4f^6 5d^1(e_g)$, termed "magnetic excitons," are formed [18,19]. Such excitons induce sharp features in the optical absorption spectrum without requiring all 5d bands to be narrow. In the absence of a direct experimental proof, the debate was never satisfactorily resolved [20,21]. In most works and reviews, the interpretation of Watcher *et al.* [17,22] is given as correct [1,3]. Only a few Japanese groups still consider the Kasuya model as correct and interpret their data accordingly [4,5,11].

In this Letter, we report the first experimental proof of the excitonic nature of the onset of the absorption spectrum in EuS. The proof is provided by the valence-to-core resonant inelastic x-ray scattering (RIXS) at the Eu L_3 edge, interpreted with the density-functional theory (DFT) and the dynamical–mean-field theory (DMFT). The RIXS process is schematically shown in Fig. 1: the absorption of an x-ray photon ω_1 excites an Eu $2p_{3/2}$ core electron to the conduction band, bringing the system into an intermediate state with a core hole that perturbs the valence electronic structure. Electrons from occupied levels in the valence-band region then fill the $2p_{3/2}$ core hole and the excess energy is released by an emission of a second x-ray photon ω_2 that is registered in a spectrometer. The result of the RIXS process is a final state with an electron transferred from the valence to the conduction band, analogous (but not identical) to what is obtained in optical spectroscopy through the absorption of a single photon in the UV-visible range.

Figure 2(a) shows the experimental RIXS of EuS collected on the ID26 beamline at the European Synchrotron Radiation Facility ([23] and Supplemental Material [24], Secs. S.I and S.II). The RIXS map reports the intensity of the ω_2 scattered x-rays as a function of the energy of the ω_1 incident x-rays and of the energy transferred to the system, that is, $\omega_1 - \omega_2$. Three main features appear at positive energy transfer: two sharp and localized features at 2.5 eV and 4.5 eV energy transfer (A and B, respectively), and a broad and extended feature centered at 9 eV energy transfer (C). By integrating the RIXS along the incident-energy axis, we are summing over all intermediate states reached by the absorption of the ω_1 photon (see Fig. 1). The resulting curve corresponds to all final states reached by the RIXS process and can be compared to the optical absorption. Figure 2(b) compares our integrated RIXS with the optical absorption spectrum of EuS from [53]. The shapes of the two curves are very close in the 1–6 eV range, and hence the two peaks at the onset of the optical absorption and features A and B of our RIXS likely correspond to the same type of excitations. The peaks in the optical and integrated RIXS spectra are slightly misaligned (by approximately 0.1 eV), which is a hint that each of them is

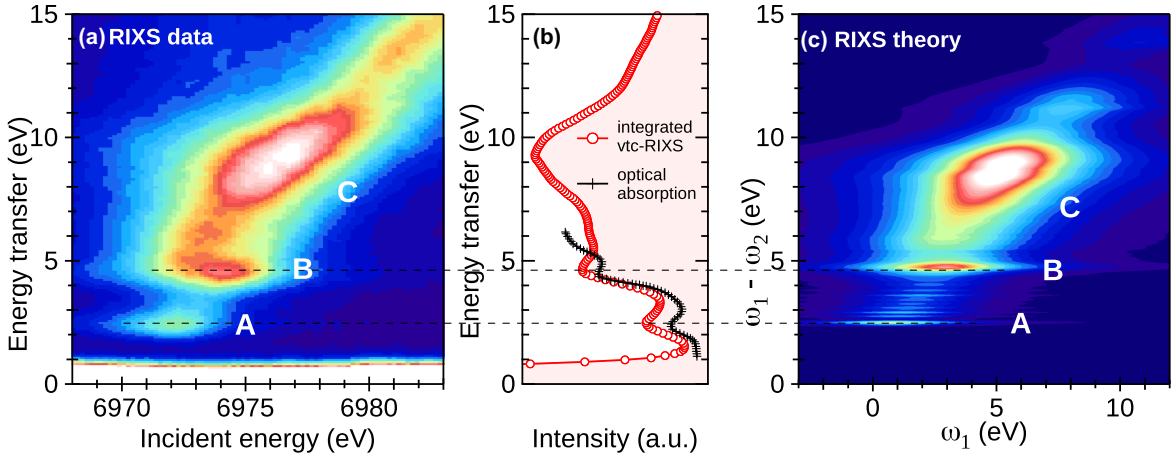

FIG. 2. (a) Experimental RIXS, (b) comparison of the optical absorption spectrum from [53] with the RIXS integrated along the incident-energy axis, and (c) calculated RIXS including the dipole (Eu 5d → Eu 2p) and quadrupole (Eu 4f → Eu 2p) emission.

composed of a group of excitations rather than of a single excitation. Differences in selection rules and in transition amplitudes governing RIXS and optical absorption cause different excitations within each group to be accentuated, which leads to an apparent shift of the corresponding spectral features when the individual excitations are not resolved. Similar misalignment of RIXS and optical features was observed for d–d transitions in VO_2 [54].

To understand the observed spectra, we modeled the RIXS process with a simplified formula proposed by Jiménez-Mier *et al.* [55] and further developed and benchmarked against experimental data by Smolentsev *et al.* [56]. When one can neglect dependence on the polarization of photons together with all many-body phenomena, such as excitonic effects possibly induced by the hole in the core level (intermediate state) or in the valence band (final state), the Kramers–Heisenberg formula [57,58] for the RIXS intensity reduces to a convolution of the unoccupied and occupied densities of states (DOSs) projected to the symmetry allowed by the electric dipole selection rules,

$$I_D \propto \int \mathrm{d}\epsilon \frac{\mathrm{DOS}_{5\mathrm{d}}^{\mathrm{occ}}(\epsilon)\mathrm{DOS}_{5\mathrm{d}}^{\mathrm{empty}}(\epsilon+\omega_1-\omega_2)}{(\epsilon-\omega_2-\epsilon_{2\mathrm{p}})^2+\Gamma_{2\mathrm{p}}^2/4}. \quad (1)$$

Here ω_1 and ω_2 are the energies of the absorbed and emitted photons, $\epsilon_{2\mathrm{p}}$ is the energy of the $2\mathrm{p}_{2/3}$ core level, and $\Gamma_{2\mathrm{p}} = 3.91$ eV is its lifetime broadening (the full width at half maximum, value adopted from [59]). The adequacy of this formula for the present application is discussed in Supplemental Material [24], Secs. S.VII and S.VIII.

We calculated the DOSs entering Eq. (1) with the DFT + DMFT method, which solves a multiband Hubbard model built on top of the DFT band structure. The Coulomb repulsion added to the Eu 4f shells is parametrized by four Slater parameters F_k, the values of which [60] were adjusted to reproduce various spectroscopies [25,26]. Apart from the limited accuracy in modeling the strongly correlated 4f electrons, DFT alone also underestimates the gap between the S 3p and Eu 5d bands. We have corrected this deficiency by empirically increasing the binding energy of the S 3p bands such that the final DFT + DMFT band structure is consistent with valence-band x-ray photoemission spectroscopy (XPS) [27] as well as with the optical absorption [17,22]. Further details of our DFT + DMFT calculations are reported in Supplemental Material [24] (Sec. S.III) where we also compare our theory with angle-resolved photoemission spectroscopy measurements [16].

The orbital-resolved spectral density calculated in the paramagnetic phase is shown in Fig. 3. It reflects the states with one electron removed from the system ($E < 0$) or with one electron added to the system ($E > 0$), and it can be experimentally probed by photoemission and inverse-photoemission spectroscopy. For uncorrelated states, the spectral density simplifies to the single-particle DOS. The

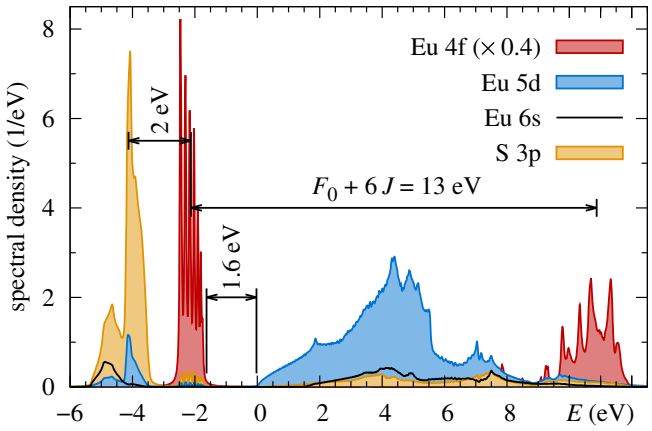

FIG. 3. Spectral density of the paramagnetic phase computed with the DFT + DMFT method. Indicated are: the distance between the S 3p bands and the Eu 4f states (2 eV) as seen in valence-band XPS [27], the optical gap between Eu 4f states and Eu 5d bands (1.6 eV) as observed in optical absorption [17], and the distance between the occupied and unoccupied 4f states (13 eV) that agrees with the estimate $F_0 + 6J$ [61], where $F_0 = 7$ eV is the first Slater parameter and $J = 1$ eV is the Hund J [60].

Eu 4f states appearing below the Fermi level in Fig. 3 consist of the $L = 3$, $S = 3$ manifold of the $4f^6$ configuration, split by the spin-orbit coupling into seven multiplets ^7F_J with $J = 0, 1, \ldots, 6$. The 4f states above the Fermi level originate predominantly from the $L = 3$, $S = 3$ manifold of the $4f^8$ configuration, and the spin-orbit multiplets ^7F_J are intermixed in this case by hybridization between the 4f states and Eu 5d and 6p bands, with which the unoccupied 4f states overlap. The Eu 5d bands are broad and spread over more than 8 eV. This shape is clearly inconsistent with the main assumption of the Wachter *et al.* interpretation of the optical spectra [17], according to which the Eu $5\mathrm{d}(t_{2g})$ and $5\mathrm{d}(e_g)$ subbands should be sharp and well separated from each other.

The RIXS calculated by means of Eq. (1) and using the 5d DOS plotted in Fig. 3 looks just like the map shown in Fig. 2(c) but with the features A and B missing (see Supplemental Material [24], Fig. S5). The feature C is nicely reproduced in the calculations. The shape of the computed RIXS follows from first principles; the energy transfer, at which the feature C is located, comes from the band gaps that were calibrated to valence XPS [27] and optical absorption [17,22]. This confirms that our RIXS is compatible with those spectroscopic measurements. Inspection of the Eu 5d DOS (Fig. 3) reveals that the $5\mathrm{d} \rightarrow 2\mathrm{p}$ emission involves mainly the Eu 5d states covalently mixed into the nominally S 3p bands. Hence, the feature C corresponds to charge-transfer excitations: the excited states contain a hole in the S 3p valence bands and an electron excited to the Eu 5d conduction band.

The theory presented so far does not reproduce the features A and B, which, therefore, cannot be due to

transitions to extended Eu 5d(t_{2g}) and 5d(e_g) band states as the popular interpretation of the optical absorption would imply. The sharpness of features A and B in the experimental RIXS and their lower excitation energy compared to the S 3p → Eu 5d charge transfer suggest that they could be bound $4f^6 5d^1$ excitons. We analyzed the expected properties of such excitons using the standard DFT combined with the open-core approximation for the 4f states [28,29] that allows us to constrain the 4f shell to a particular filling, $4f^6$ or $4f^7$ (see Supplemental Material [24], Secs. S.IV and S.V).

The excitons were modeled in supercells (the largest we could afford was $4 \times 4 \times 4$ multiple of the EuS conventional cell, that is, 512 atoms), in which one of the Eu atoms was constrained to have the $4f^6$ configuration and the remaining electron was transferred to the conduction bands. This is analogous to the constrained self-consistent field method called excited-electron and core-hole (XCH) approximation sometimes used to model core-hole effects in x-ray absorption spectra [62–65]. The excited electron turns out to remain bound near the 4f hole; the valence charge density integrated over a sphere with radius $3.1 r_{\mathrm{Bohr}}$ around the perturbed atom contains approximately half of an electron more than the same sphere centered at a bulk Eu site. Figure 4 compares the DOS projected on the 5d states at the atom with the 4f hole to the 5d DOS of the unperturbed bulk. The open-core bulk DOS is almost identical to the DFT + DMFT DOS plotted in Fig. 3. The local 5d DOS at the excited atom substantially deviates from the bulk 5d DOS: it consists of two distinguished sharp peaks, one of t_{2g} and the other of e_g character, each having a weak tail extending toward high energies. The maxima of these peaks are 2 eV apart, just like the excitation energies of the RIXS features A and B.

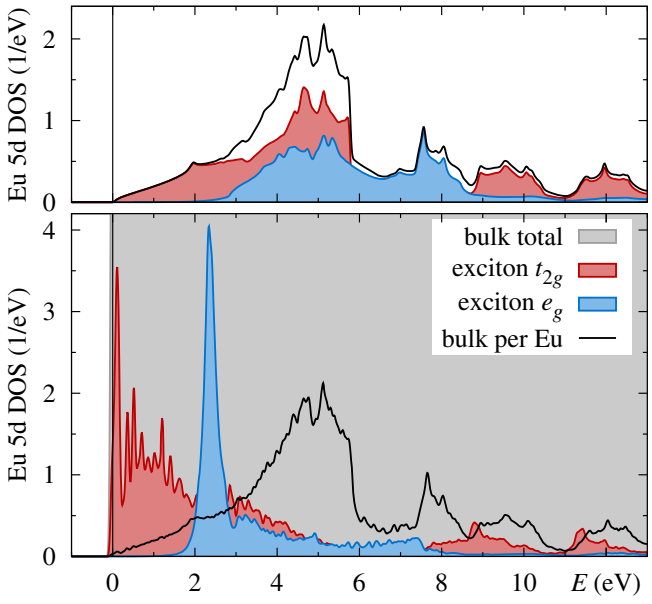

FIG. 4. Unoccupied Eu 5d DOS computed in the open-core approximation and decomposed into its e_g (blue) and t_{2g} (red) components. The bulk DOS computed in the primitive cell (top) is compared to the local DOS at the excited atom placed in the $4 \times 4 \times 4$ supercell (bottom). The grey area depicts the total 5d DOS in the supercell and indicates that the excitons overlap with these bulk states.

To estimate how the computed excitons would show up in the RIXS plane, we employ a formula analogous to Eq. (1),

$$I_Q \propto \int \mathrm{d}\epsilon \frac{n_{4f}\delta(\epsilon+\Delta)\mathrm{DOS}^{\mathrm{empty}}_{5d\,\mathrm{exc}}(\epsilon+\omega_1-\omega_2)}{(\epsilon-\omega_2-\epsilon_{2p})^2+\Gamma^2_{2p}/4}, \quad (2)$$

where the occupied DOS is now the 4f DOS, for simplicity approximated by a single peak, $n_{4f}\delta(\epsilon+\Delta)$, and the unoccupied DOS is the local 5d DOS at the atom containing the exciton (Fig. 4). Placing the occupied 4f states at the binding energy $-\Delta$ ensures that the lowest exciton appears at the energy transfer equal Δ (the unoccupied exciton DOS starts at the Fermi level chosen as the energy reference, $E_F = 0$). This adjustment of the 4f-state position can be understood as a many-body correction introducing the exciton binding energy into the single-particle theory, which was used to derive Eq. (1). To compute Δ, we evaluate the total energy of the unperturbed supercell with all atoms in the $4f^7$ configuration, E_{clean}, and the total energy of the supercell with one Eu atom constrained to have the $4f^6$ configuration, E_{exc}. We find $\Delta = E_{\mathrm{exc}} - E_{\mathrm{clean}} = 2.4$ eV, very close to the excitation energy of the RIXS feature A.

Using the occupied 4f DOS in place of the occupied DOS in Eq. (2) implies that the emission of the ω_2 photon is due to quadrupole 4f → 2p transition, which has a much smaller intensity than the dipole 5d → 2p transition assumed in Eq. (1). When combining the contributions of Eqs. (1) and (2) in Fig. 2(c), we assume that the ratio of quadrupolar to dipolar emission probabilities, $p_Q/p_D = 0.024$, is the same as the ratio of the corresponding absorption probabilities deduced from absorption data ([30] and Supplemental Material [24], Sec. S.VI). The counterintuitive finding of the dipolar and quadrupolar features having comparable intensity in the final RIXS map stems from the very different number of the occupied states: there are seven occupied 4f states available to decay through the quadrupole channel, whereas only about 0.6 occupied 5d states (the integral over the occupied 5d DOS in Fig. 3) are available to decay through the dipole channel. This results in a large enhancement of the quadrupole contribution, $n_{4f}/n_{5d} = 11.7$, partly canceling its small emission probability. An analogously enhanced emission from an occupied 4f shell was observed in the $L_{2,3}$ RIXS of Re and W oxides [56]. It is conceivable that in more ionic compounds like halides, which have even smaller covalent admixture of the 5d states in the ligand bands, the quadrupole RIXS features are even dominant.

The final theoretically derived RIXS map is shown in Fig. 2 side by side with the experimental RIXS. The excellent agreement of the shape and energy position of all features between experiment and theory provides a convincing argument for our interpretation of the RIXS of EuS, and it ultimately demonstrates that the peaks A and B are the $4f^6 5d^1(t_{2g})$ and $4f^6 5d^1(e_g)$ localized excitons proposed by Kasuya and collaborators. These excitons *are not* incompatible with the finite photoconductivity observed in EuS since they overlap with the itinerant 5d band states (Fig. 4) and can, therefore, decay into them. This decay generates mobile charge carriers necessary for the photocurrent to occur [21,22].

We can compare our findings with a recent study by Joos *et al.* [66] who use multiconfigurational *ab inito* embedded-cluster methods to investigate the Eu^{2+} excited-state landscape in Eu-doped alkaline-earth sulfides MS (M = Ca, Sr, Ba), which have the same rock salt structure as EuS. The optical absorption spectra of these doped sulfides are characterized by two peaks, which were shown to correspond to the spin-allowed electric-dipole transitions toward the excited $4f^6 5d^1(t_{2g})$ and $4f^6 5d^1(e_g)$ manifolds of Eu^{2+}. Both these bands posses a complex fine structure about 1 eV wide that originates from term and multiplet splitting due to the 4f–5d Coulomb interaction and the spin-orbit coupling. Given the structural and chemical similarities of EuS and MS:Eu^{2+}, it can be presumed that a similar fine structure is present under features A and B in Fig. 2, but it is hidden below the experimental resolution. At present, this fine structure is manifested only indirectly by a misalignment between the optical absorption and RIXS spectra (Fig. 2) as discussed above.

In conclusion, we combined RIXS experiments with electronic-structure calculations to settle a long-standing debate on the nature of low-energy electronic excitations in the magnetic semiconductor EuS. It was evidenced that so-called magnetic excitons, composed of a hole and an electron localized in atomic-like 4f and 5d orbitals of a single Eu^{2+} ion, are formed at excitation energies of 2.5 and 4.5 eV. These excitonic states correspond to the crystal-field-split $4f^6 5d^1$ manifolds that are known from optical spectroscopy of isolated Eu^{2+} impurities.

Acknowledgments—Authors acknowledge the ESRF for providing beamtime. Computational resources were provided by the e-INFRA CZ project (ID: 90254), supported by the Ministry of Education, Youth and Sports of the Czech Republic. L. A. acknowledges support from the European Research Council (ERC) under Grant No. 759696. J. K. acknowledges financial support by the Czech Science Foundation under the Grant No. 21-09766S. J. J. J. acknowledges the Ghent University Special Research Fund via Project No. BOF/PDO/2017/002101.

Data availability—The input files for the electronic structure calculations as well as the output data used to plot the figures in this Letter and in Supplemental Material [24] are deposited at [67]. The in-house software that can be made publicly available at the time of publication of this Letter is deposited at [68].

[1] A. Mauger and C. Godart, The magnetic, optical, and transport properties of representatives of a class of magnetic semiconductors: The europium chalcogenides, Phys. Rep. **141**, 51 (1986).
[2] B. T. Matthias, R. M. Bozorth, and J. H. Van Vleck, Ferromagnetic interaction in EuO, Phys. Rev. Lett. **7**, 160 (1961).
[3] V. M. Huxter, T. Mirkovic, P. S. Nair, and G. D. Scholes, Demonstration of bulk semiconductor optical properties in processable Ag_2S and EuS nanocrystalline systems, Adv. Mater. **20**, 2439 (2008).
[4] Y. Hasegawa, Magnetic semiconductor EuO, EuS, and EuSe nanocrystals for future optical devices, Chem. Lett. **42**, 2 (2013).
[5] Y. Hasegawa and T. Nakanishi, Europium chalcogenide nanoparticles, in *Handbook on the Physics and Chemistry of Rare Earths* (Elsevier, New York, 2015), Vol. 47, pp. 101–146, 10.1016/B978-0-444-63481-8.00270-0.
[6] D. R. C. Asuigui, M. C. De Siena, R. Fainblat, D. James, D. R. Gamelin, and S. L. Stoll, Giant band splittings in EuS and EuSe magnetic semiconductor nanocrystals, Chem. Commun. (Cambridge) **56**, 5843 (2020).
[7] F. Katmis, V. Lauter, F. S. Nogueira, B. A. Assaf, M. E. Jamer, P. Wei, B. Satpati, J. W. Freeland, I. Eremin, D. Heiman, P. Jarillo-Herrero, and J. S. Moodera, A high-temperature ferromagnetic topological insulating phase by proximity coupling, Nature (London) **533**, 513 (2016).
[8] R. T. Lechner, G. Springholz, T. U. Schülli, J. Stangl, T. Schwarzl, and G. Bauer, Strain induced changes in the magnetic phase diagram of metamagnetic heteroepitaxial $EuSe/PbSe_{1-x}Te_x$ multilayers, Phys. Rev. Lett. **94**, 157201 (2005).
[9] N. J. C. Ingle and I. S. Elfimov, Influence of epitaxial strain on the ferromagnetic semiconductor EuO: First-principles calculations, Phys. Rev. B **77**, 121202(R) (2008).
[10] M. Matsubara, A. Schroer, A. Schmehl, A. Melville, C. Becher, M. Trujillo-Martinez, D. G. Schlom, J. Mannhart, J. Kroha, and M. Fiebig, Ultrafast optical tuning of ferromagnetism via the carrier density, Nat. Commun. **6**, 6724 (2015).
[11] M. Matsubara, Ultrafast optical control of magnetic interactions in carrier-density-controlled ferromagnetic semiconductors, Appl. Sci. **9**, 948 (2019).
[12] V. N. Kats, L. A. Shelukhin, P. A. Usachev, D. V. Averyanov, I. A. Karateev, O. E. Parfenov, A. N. Taldenkov, A. M. Tokmachev, V. G. Storchak, and V. V. Pavlov, Femtosecond optical orientation triggering magnetization precession in epitaxial EuO films, Nanoscale **15**, 2828 (2023).
[13] N. M. Souza-Neto, D. Haskel, Y.-C. Tseng, and G. Lapertot, Pressure-induced electronic mixing and enhancement of

ferromagnetic ordering in EuX (X = Te, Se, S, O) magnetic semiconductors, Phys. Rev. Lett. **102**, 057206 (2009).
[14] H. Miyazaki, T. Ito, H. J. Im, S. Yagi, M. Kato, K. Soda, and S. Kimura, Direct observation of momentum-dependent exchange interaction in a Heisenberg ferromagnet, Phys. Rev. Lett. **102**, 227203 (2009).
[15] J. M. Riley, F. Caruso, C. Verdi, L. B. Duffy, M. D. Watson, L. Bawden, K. Volckaert, G. van der Laan, T. Hesjedal, M. Hoesch, F. Giustino, and P. D. C. King, Crossover from lattice to plasmonic polarons of a spin-polarised electron gas in ferromagnetic EuO, Nat. Commun. **9**, 2305 (2018).
[16] A. V. Fedorov, G. Poelchen, S. V. Eremeev, S. Schulz, A. Generalov, C. Polley, C. Laubschat, K. Kliemt, N. Kaya, C. Krellner, E. V. Chulkov, K. Kummer, D. Yu. Usachov, A. Ernst, and D. V. Vyalikh, Insight into the temperature evolution of electronic structure and mechanism of exchange interaction in EuS, J. Phys. Chem. Lett. **12**, 8328 (2021).
[17] G. Güntherodt, P. Wachter, and D. M. Imboden, Energy level scheme and the effect of magnetic order on the optical transitions in europium chalcogenides, Phys. Kondens. Mater. **12**, 292 (1971).
[18] T. Kasuya and A. Yanase, Anomalous transport phenomena in Eu-chalcogenide alloys, Rev. Mod. Phys. **40**, 684 (1968).
[19] T. Kasuya, S-f exchange interactions and magnetic semiconductors, Crit. Rev. Solid State Sci. **3**, 131 (1972).
[20] T. Kasuya, Photoluminescence and absorption mechanisms in Eu monochalcogenides, J. Magn. Magn. Mater. **195**, 141 (1999).
[21] P. Wachter and B. Bucher, Exciton condensation and its influence on the specific heat, Physica (Amsterdam) **408B**, 51 (2013).
[22] P. Wachter, The optical electrical and magnetic properties of the europium chalcogenides and the rare earth pnictides, Crit. Rev. Solid State Sci. **3**, 189 (1972).
[23] P. Glatzel, A. Harris, P. Marion, M. Sikora, T.-C. Weng, C. Guilloud, S. Lafuerza, M. Rovezzi, B. Detlefs, and L. Ducotté, The five-analyzer point-to-point scanning crystal spectrometer at ESRF ID26, J. Synchrotron Radiat. **28**, 362 (2021).
[24] See Supplemental Material at http://link.aps.org/supplemental/10.1103/PhysRevLett.134.046401 for details on (i) sample synthesis, (ii) RIXS instrumentation and measurements, (iii) LDA + DMFT calculations, (iv) open-core LDA calculations, (v) modeling the localized excitons in supercells using the open-core approximation, (vi) estimation of the intensity of the 4f → 2p quadrupolar emission, (vii) indirect RIXS processes, and (viii) influence of intershell Coulomb interaction on the RIXS spectra. Supplemental Material includes Refs. [16,22,23,25–52].
[25] H. Ogasawara, A. Kotani, and B. T. Thole, Lifetime effect on the multiplet structure of 4d x-ray-photoemission spectra in heavy rare-earth elements, Phys. Rev. B **50**, 12332 (1994).
[26] I. L. M. Locht, Y. O. Kvashnin, D. C. M. Rodrigues, M. Pereiro, A. Bergman, L. Bergqvist, A. I. Lichtenstein, M. I. Katsnelson, A. Delin, A. B. Klautau, B. Johansson, I. Di Marco, and O. Eriksson, Standard model of the rare earths analyzed from the Hubbard I approximation, Phys. Rev. B **94**, 085137 (2016).
[27] P. Cotti and P. Munz, Photoemissionsmessungen an Europiumchalkogeniden, Phys. Condens. Matter **17**, 307 (1974).
[28] S. K. Malik, F. J. Arlinghaus, and W. E. Wallace, Spin-polarized energy-band structure of YCo_5, $SmCo_5$, and $GdCo_5$, Phys. Rev. B **16**, 1242 (1977).
[29] M. S. S. Brooks, L. Nordström, and B. Johansson, 3d-5d band magnetism in rare earth-transition metal intermetallics: Total and partial magnetic moments of the RFe_2 (R = Gd-Yb) Laves phase compounds, J. Phys. Condens. Matter **3**, 2357 (1991).
[30] F. Bartolomé, M. H. Krisch, D. Raoux, and J.-M. Tonnerre, Quadrupolar excitation channels at the L_3 edge of rare-earth ions probed by resonant inelastic x-ray scattering, Phys. Rev. B **60**, 13497 (1999).
[31] L. J. P. Ament, F. Forte, and J. van den Brink, Ultrashort lifetime expansion for indirect resonant inelastic x-ray scattering, Phys. Rev. B **75**, 115118 (2007).
[32] J. M. An, S. V. Barabash, V. Ozolins, M. van Schilfgaarde, and K. D. Belashchenko, First-principles study of phase stability of Gd-doped EuO and EuS, Phys. Rev. B **83**, 064105 (2011).
[33] J. van den Brink and M. van Veenendaal, Theory of indirect resonant inelastic x-ray scattering, J. Phys. Chem. Solids **66**, 2145 (2005).
[34] B. Chatterjee and J. Kolorenč, Electronic structure and magnetism in UGa_2: DFT + DMFT approach, Phys. Rev. B **103**, 205146 (2021).
[35] R. D. Cowan, *The Theory of Atomic Structure and Spectra* (University of California Press, Berkeley, 1981).
[36] A. Georges, G. Kotliar, W. Krauth, and M. J. Rozenberg, Dynamical mean-field theory of strongly correlated fermion systems and the limit of infinite dimensions, Rev. Mod. Phys. **68**, 13 (1996).
[37] G. Y. Guo, H. Ebert, W. M. Temmerman, K. Schwarz, and P. Blaha, Relativistic effects on the structural and magnetic properties of iron, Solid State Commun. **79**, 121 (1991).
[38] A. Hariki, M. Winder, T. Uozumi, and J. Kuneš, LDA + DMFT approach to resonant inelastic x-ray scattering in correlated materials, Phys. Rev. B **101**, 115130 (2020).
[39] M. W. Haverkort, G. Sangiovanni, P. Hansmann, A. Toschi, Y. Lu, and S. Macke, Bands, resonances, edge singularities and excitons in core level spectroscopy investigated within the dynamical mean-field theory, Europhys. Lett. **108**, 57004 (2014).
[40] M. W. Haverkort, Quanty for core level spectroscopy—excitons, resonances and band excitations in time and frequency domain, J. Phys. Conf. Ser. **712**, 012001 (2016).
[41] J. J. Joos, D. Poelman, and P. F. Smet, Energy level modeling of lanthanide materials: Review and uncertainty analysis, Phys. Chem. Chem. Phys. **17**, 19058 (2015).
[42] J. Kolorenč, A. B. Shick, and A. I. Lichtenstein, Electronic structure and core-level spectra of light actinide dioxides in the dynamical mean-field theory, Phys. Rev. B **92**, 085125 (2015).
[43] J. Kolorenč, Theory of resonant x-ray emission spectra in compounds with localized f electrons, Physica (Amsterdam) **536B**, 695 (2018).
[44] A. Kotani, K. O. Kvashnina, S. M. Butorin, and P. Glatzel, Spectator and participator processes in the resonant

photon-in and photon-out spectra at the Ce L_3 edge of CeO_2, Eur. Phys. J. B **85**, 257 (2012).
[45] A. A. Mostofi, J. R. Yates, Y.-S. Lee, I. Souza, D. Vanderbilt, and N. Marzari, Wannier90: A tool for obtaining maximally-localised Wannier functions, Comput. Phys. Commun. **178**, 685 (2008).
[46] L. Nordström, B. Johansson, and M. S. S. Brooks, Calculation of the electronic structure and the magnetic moments of $Nd_2Fe_{14}B$, J. Phys. Condens. Matter **5**, 7859 (1993).
[47] M. Schlipf, M. Betzinger, M. Ležaić, C. Friedrich, and S. Blügel, Structural, electronic, and magnetic properties of the europium chalcogenides: A hybrid-functional DFT study, Phys. Rev. B **88**, 094433 (2013).
[48] D. Sheets, V. Flynn, J. Kim, M. Upton, D. Casa, T. Gog, Z. Fisk, M. Dzero, P. F. S. Rosa, D. G. Mazzone, I. Jarrige, J.-X. Zhu, and J. Hancock, Exploring itinerant states in divalent hexaborides using rare-earth L edge resonant inelastic x-ray scattering, J. Phys. Condens. Matter **32**, 135601 (2019).
[49] I. Souza, N. Marzari, and D. Vanderbilt, Maximally localized Wannier functions for entangled energy bands, Phys. Rev. B **65**, 035109 (2001).
[50] M. van Veenendaal, *Theory of Inelastic Scattering and Absorption of X-Rays* (Cambridge University Press, Cambridge, United Kingdom, 2015).
[51] P. Blaha, K. Schwarz, F. Tran, R. Laskowski, G. K. H. Madsen, and L. D. Marks, WIEN2k: An APW + lo program for calculating the properties of solids, J. Chem. Phys. **152**, 074101 (2020).
[52] WIEN2k-FAQ:, "open core" treatment of 4(5)f electrons (2001), http://www.wien2k.at/reg_user/faq/open_core.html.
[53] P. Poulopoulos, B. Lewitz, A. Straub, S. D. Pappas, S. A. Droulias, S. Baskoutas, and P. Fumagalli, Band-gap tuning at the strong quantum confinement regime in magnetic semiconductor EuS thin films, Appl. Phys. Lett. **100**, 211910 (2012).
[54] L. Braicovich, G. Ghiringhelli, L. H. Tjeng, V. Bisogni, C. Dallera, A. Piazzalunga, W. Reichelt, and N. B. Brookes, Neutral 3d excitations in insulating VO_2 as seen with resonant inelastic x-ray scattering at the V $L_{3,2}$ edges, Phys. Rev. B **76**, 125105 (2007).
[55] J. Jiménez-Mier, J. van Ek, D. L. Ederer, T. A. Callcott, J. J. Jia, J. Carlisle, L. Terminello, A. Asfaw, and R. C. Perera, Dynamical behavior of x-ray absorption and scattering at the L edge of titanium compounds: Experiment and theory, Phys. Rev. B **59**, 2649 (1999).
[56] N. Smolentsev, M. Sikora, A. V. Soldatov, K. O. Kvashnina, and P. Glatzel, Spin-orbit sensitive hard x-ray probe of the occupied and unoccupied 5d density of states, Phys. Rev. B **84**, 235113 (2011).
[57] H. A. Kramers and W. Heisenberg, Über die Streuung von Strahlung durch Atome, Z. Phys. **31**, 681 (1925).
[58] J. W. Sakurai, *Advanced Quantum Mechanics* (Addison-Wesley, Reading, MA, 1967), pp. 47–50, 53–57.
[59] M. O. Krause and J. H. Oliver, Natural widths of atomic K and L levels, Kα x-ray lines and several KLL Auger lines, J. Phys. Chem. Ref. Data **8**, 329 (1979).
[60] We use $F_0 = 7.0$ eV, $F_2 = 12.1$ eV, $F_4 = 7.7$ eV, and $F_6 = 5.5$ eV, which correspond to Hubbard $U = 7.0$ eV and Hund $J = 1.0$ eV.
[61] D. van der Marel and G. A. Sawatzky, Electron-electron interaction and localization in d and f transition metals, Phys. Rev. B **37**, 10674 (1988).
[62] K. A. Jackson and M. R. Pederson, New theoretical model for the diamond 1s core exciton, Phys. Rev. Lett. **67**, 2521 (1991).
[63] S.-D. Mo and W. Y. Ching, *Ab initio* calculation of the core-hole effect in the electron energy-loss near-edge structure, Phys. Rev. B **62**, 7901 (2000).
[64] G. S. Michelitsch and K. Reuter, Efficient simulation of near-edge x-ray absorption fine structure (NEXAFS) in density-functional theory: Comparison of core-level constraining approaches, J. Chem. Phys. **150**, 074104 (2019).
[65] B. P. Klein, S. J. Hall, and R. J. Maurer, The nuts and bolts of core-hole constrained *ab initio* simulation for K-shell x-ray photoemission and absorption spectra, J. Phys. Condens. Matter **33**, 154005 (2021).
[66] J. J. Joos, P. F. Smet, L. Seijo, and Z. Barandiarán, Insights into the complexity of the excited states of Eu-doped luminescent materials, Inorg. Chem. Front. **7**, 871 (2020).
[67] L. Amidani, J. J. Joos, P. Glatzel, and J. Kolorenč, Zenodo, 10.5281/zenodo.14170326.
[68] J. Kolorenč, Zenodo, 10.5281/zenodo.14192968.